UC Davis

UC Davis Previously Published Works

Title

Nanoporous ultra-high specific surface inorganic fibres

Permalink

https://escholarship.org/uc/item/5rx8106j

Journal

Nanotechnology, 18

ISSN

0957-4484

Authors

Ding, Bin
Kanehata, Masaki
Shiratori, Seimei

Publication Date

2007-08-01

Peer reviewed

eScholarship.org Powered by the California Digital Library
University of California

Nano-porous ultra-high specific surface inorganic fibers

Masaki Kanehata[1], Bin Ding[2,3] and Seimei Shiratori[1,3]

[1] Faculty of Science and Technology, Keio University, Yokohama 223-8522, Japan

[2] Fiber and Polymer Science, University of California, Davis, CA 95616, USA

[3] Corresponding authors.

E-mail: bding@ucdavis.edu and shiratori@appi.keio.ac.jp

Abstract

Nano-porous inorganic (silica) nanofibers with ultra-high specific surface have been fabricated by electrospinning the blend solutions of poly(vinyl alcohol) (PVA) and colloidal silica nanoparticles, followed by selective removal of the PVA component. The configurations of the composite and inorganic nanofibers were investigated by changing the average silica particle diameters and the concentrations of colloidal silica particles in polymer solutions. After the removal of PVA by calcination, the fiber shape of pure silica particle assembly was maintained. The nano-porous silica fibers were assembled as a porous membrane with a high surface roughness. From the results of Brunauer-Emmett-Teller (BET) measurements, the BET surface area of inorganic silica nanofibrous membranes was increased with the decrease of the particle diameters. The membrane composed of silica particles with diameter of 15 nm showed the largest BET surface area of 270.3 m^2g^{-1} and total pore volume of 0.66 cm^3g^{-1}. The physical absorption of methylene blue dye molecules by nano-porous silica membranes was examined using UV-vis spectrometer. Additionally, the porous silica membranes modified with fluoroalkylsilane showed the super-hydrophobicity due to their porous structures.

1. Introduction

In recent years, porous materials have been of immense interest because of their potential for applications in fuel cell membranes, tissue engineering, catalysis, sensors, separations, electrochemical cells, drug delivery, chemical filtration, etc [1-6]. Porous SiO_2 with controlled porosity and high specific surface is strongly required as it offers great potential applications such as sensors, electroluminescence materials, photovoltaic materials, etc [7-9].

On the other hand, the nanofibers prepared by electrospinning method have been intensively studied for its unique properties [10] and potential applications such as sensors [4, 5], filters [6], dye-sensitized solar cells [11, 12], tissue engineering [2], and super-hydrophobic materials [13, 14]. The process of electrospinning is a special case of the electrospray process which uses electrostatic fields to form and accelerate a liquid jet from the tip of a capillary [15].

Many applications of electrospun nanofibers could be greatly improved by increasing the surface area and porosity of the fibers. Towards that aim, a number of groups have tried to produce porous nanofibers in a versatile and inexpensive way. As a typical method, the electrospun porous polymer nanofibers can be obtained by selective dissolution [2, 16-18] or calcination [19-21] for the removal of one phase from fibers with multi-phase. Recently, Xia et al [22] reported that, by immersing the collector in a bath of liquid nitrogen, porous polymer fibers can be fabricated through thermally induced phase separation between the solvent-rich and solvent-poor regions in the fiber during electrospinning, followed by removal of solvent in vacuo. Additionally, the fabrication of nano-porous carbon fibers was reported by the electrospinning two immiscible polymer solutions followed by thermal

treatment at elevated temperature in an inert atmosphere [23, 24].

The electrospun inorganic nanofibers containing SiO_2 componenet have been reported by electrospinning the polymer with sol-gel solution [20, 25], sol-gel solution [26], and polymer solution blended with colloidal silica particles [27], respectively. However, to our best knowledge, the SiO_2 nanofibers with ultra-high surface area and porosity are difficult to find in periodicals and monographs.

In this study, we want to fabricate the highly porous SiO_2 nanofibers with ultra-high surface area and porosity. The water-soluble poly (vinyl alcohol) (PVA) can be introduced as template material [28] to blend with colloidal silica nanoparticles for preparing the composite nanofibers. Inorganic silica nanofibers could be obtained by the calcination of the composite fibers. The morphology, surface area, fiber pore diameter, and total pore volume of fibrous samples were studied upon the average diameters of silica nanoparticles and concentrations of silica in polymer solutions. Moreover, the absorption of methylene blue (MB) dye by fibrous silica membranes and the hydrophobicity of fluoroalkylsilane (FAS) modified fibrous silica membranes were also investigated.

2. Experimental

Colloidal silica nanoparticles (STS, Nissan Chemical Industries, Ltd.) with the average particle diameters of 15, 50, and 100 nm were dispersed in water with a silica concentration of 20 wt%. The template PVA (M_n 66 000, Wako) was dissolved into water with a PVA concentration of 10 wt% at 80 ^oC under stirring. Then, the electrospinning solutions were obtained by blending colloidal silica and PVA solutions with a silica/PVA solution weight ratio of 2/3. To fix the concentration of PVA in all electrospinning solutions, the 10 wt% of PVA solution was diluted to 6 wt%. The detailed compositions of electrospinning solutions

were listed in Table 1.

The electrospinning solution was transferred into a 20 ml plastic syringe. Then, the syringe was fixed on a syringe pump (MSP-DT2, As One, Ltd.). The feeding rate of solution by syringe pump was 1 mlh^{-1}. The positive electrode of a high voltage power supply (FC30P4, Glassman High Voltage Inc., USA) was connected with metal tip, which connected with plastic syringe. A grounded stainless tubular layer which covered by a piece of aluminum foil was used as fiber collector. The applied voltage was 10 kV, and tip-to-collector distance was 10 cm. The ambient temperature and relative humidity was kept at 25 □ and 50 %, respectively. The detail of the electrospinning process is described in our previous report [14]. The fibrous membranes were obtained on the surface of collector. The fibrous membranes were calcined at 450 □ in air for 2 h to remove the PVA. The composite fibers containing the average particle diameters of 15, 50, and 100 nm were denoted as PVA/SiO_2(15), PVA/SiO_2(50), and PVA/SiO_2(100), respectively. The calcined samples of PVA/SiO_2(15), PVA/SiO_2(50), and PVA/SiO_2(100) fibers were referred to as SiO_2(15), SiO_2(50), and SiO_2(100), respectively.

The absorption property of fibrous silica membranes was examined by the absorption of MB (Kanto Chemical Co., Inc.) in water. For a typical procedure, 100 mg fibrous silica samples were immersed into a 5 ml MB dye solution (0.1 mM) for 2 days at 25 ^oC. The color change of MB solutions, as indicative of absorption property of porous silica membranes, was examined with UV-vis spectrometer (UV mini-1240, Shimazu).

In order to compare the hydrophobicity of FAS-modified fibrous and flat silica surfaces, a silica film was prepared with a sol-gel method [29]. The sol-gel was prepared by the hydrolysis and condensation of 25 g tetraethoxysilane (TEOS) in the mixture of 37.6 g

ethanol, 23.5 g distilled water, and 0.3 g hydrochloric acid (35 wt%). A slide glass was immersed into the sol-gel and pull out with a speed of 1 mms^{-1}. The films were dried at 80 ^{o}C for 1 h. After that, the resultant samples were modified with a 3 wt% FAS ($CF_3(CF_2)_7(CH_2)_2Si(OCH_3)_3$, GE Toshiba Silicone Co., Ltd., Japan) in hexane for 24 h at 25 ^{o}C [30]. Then, the samples were dried in air and heated at 100 ^{o}C for 1 h in an oven.

Fourier transform infrared (FT-IR) spectra were recorded using a BIO-RAD spectrometer (FTS-60A/896) in the wave number range of 4000-400 cm^{-1} at room condition. The morphologies of resultant samples were examined by field emission scanning electron microscopy (FE-SEM) and field emission transmission electron microscopy (FE-TEM). The diameters of fibers were measured using an image analyzer. The diameter of beads has not been included in the fiber diameter calculations. Surface area measurements were carried out using the BET nitrogen adsorption method with a Micromeritics ASAP 2010 apparatus. The water contact and water-roll angles of resultant samples were measured with a contact angle meter (FACE, Kyowa Interface Science Co., Ltd).

3. Results and discussion

FT-IR spectra of various samples are presented in figure 1. Figure 1a shows the FT-IR spectra of pure PVA nanofibrous membrane. A number of absorption features appeared at 3400 cm^{-1} (—OH), 2900 cm^{-1} ($—CH_2$), 1740 cm^{-1} (C=O), 1450 cm^{-1} (O=C—OR), 1340 cm^{-1} ($—CH_2$), and 1110 cm^{-1} (C—O—C), respectively [31]. As seen in figure 1b, the silica nanoparticles showed the absorption features at 1670, 1100, 790, and 470 cm^{-1} corresponding to $\upsilon_{Si—O—Si}$ [25]. The composite PVA/SiO_2 fibers (figure 1c) showed two absorption features around 2900 and 1740 cm^{-1} indicating the existence of $—CH_2$ and

C=O groups in the composite fibers. Other absorption features of PVA were overlapped by the strong absorption features of silica appeared around 1100, 790, 470 cm^{-1}, respectively. After calcination the composite fibers (figure 1d), two absorption features around 2900 and 1740 cm^{-1} disappeared, and the absorption feature around 1670 cm^{-1} became evident. This illustrated that the PVA decomposed. Additionally, it was found that the calcined sample (figure 1d) showed the same absorption features as the silica nanoparticles (figure 1b). As a result, the calcined sample was composed of silica only. Moreover, the broad peak around 3400 cm^{-1} was observed for both silica nanoparticles and silica nanofibers, showing that the moisture was absorbed by silica samples in air. The intensity of this peak can be affected by the quantity of moisture absorbed by silica samples.

The FE-SEM image of pure PVA fibrous membrane is shown in figure 2a. The PVA fibers were randomly oriented as a porous membrane. It has an average fiber diameter of 154 nm with a smooth surface. The solution properties and fiber diameters are listed in Table 1. Figure 2b provides the morphology of composite fibers containing silica particles (8 wt%) with an average particle diameter of 15 nm. After adding the silica particles in electrospinning solutions, the fiber diameter of PVA/SiO_2(15) was increased to 200 nm. Additionally, the fiber beads were observed along the fibers. The FE-SEM image of PVA/SiO_2(50) is shown in figure 1c. It has an average fiber diameter of 193 nm. Meanwhile, the grain-like particles, called the secondary structure of fibers, were appeared on the fiber surface. The composite PVA/SiO_2(100) (figure 2d) showed the thinnest fiber diameter of 172 nm among three kinds of composite fibers. The silica nanoparticles (100 nm) were singly aligned along the fiber orientations. The average thickness of PVA coating layer on particle surface could be calculated about 36 nm. For all three kinds of composite

fibers, the silica nanoparticles were embedded in the PVA nanofibers. The roughness and grain-like particles appeared on the composite fiber surface was caused by the adding of silica particles, and was adjustable with changing the average particle diameters. Additionally, as shown in Table 1, the average diameters of fibers were found strongly affected by the solution viscosities. The fiber diameters increased concurrently with the increase of the solution viscosities.

Figure 3 shows the FE-SEM images of calcined samples from the composite fibers. The SiO_2(15) fibers, as shown in figure 3a, maintained the fiber bead morphology from the PVA/SiO_2(15) fibers (figure 2b). It has an average fiber diameter of 197 nm which was similar to that (200 nm) of PVA/SiO_2(15) fibers. Obviously, the fibers were found to be composed of the nanoparticles (15 nm) and pores on fiber surface. Figure 3b gives the morphology of SiO_2(50) fibers. It has an average diameter of 188 nm. Meanwhile, the fibers also showed to be composed of silica particles (50 nm) and pores. The close-packed assembly of silica particles was obtained after calcination with using the silica particle with diameters of 15 and 50 nm. It can be observed from figure 3c, the SiO_2(100) fibers were not continuous. The fibers were broken and aggregated during the calcination process. The single particle strings were found upon the connection of aligned single silica particles which corresponded to the SEM image shown in figure 2d.

The TEM images of SiO_2(15) and SiO_2(50) fibers are shown in figure 4. As observed in figure 4a, the silica nanoparticles with an average diameter of 15 nm were found to be uniformly dispersed in the fibers. The diameter of silica particles did not increase even after the calcination at 450 ^{o}C. Moreover, a number of cavities were observed among the silica nanoparticles which attribute to increase the fiber surface area and porosity. In figure

4b, the silica particles with an average diameter of 50 nm were assembled densely into fibers. As a result, the calcined fibers were found to be highly porous throughout the fibers. Such fibers would show a much higher surface area than other smooth fibers.

The BET surface areas, pore diameters, and total pore volumes of inorganic porous silica fibers are shown in Table 2. The SiO_2(15) fibers have the largest BET surface area of 270.3 m^2g^{-1}, the smallest pore diameter of 8.8 nm, and the largest total pore volume of 0.66 cm^3g^{-1} among three samples. The porous fibers composed of colloidal silica nanoparticles showed much larger surface area than that of the inorganic fibers prepared with sol-gel [20]. Additionally, the BET surface areas and total pore volumes were found to be increased on decreasing the silica particle diameters. Therefore, the surface area of silica fibers could be further increased with decreasing the diameter of silica particles.

The physical absorption of MB dye molecules from aqueous solution has been studied by activated carbon and silica [32-34]. The preliminary absorption testing was carried out by immersion 100 mg fibrous silica membranes in a 5 ml MB (1 mM) aqueous solution. The color change of MB solutions is shown in figure 5a. It can be easily found that the color in solutions was lighten after the treatment with various fibrous silica samples. And the color was lighten gradually with decreasing the silica particle diameters. As judging from the BET surface area measurements, the BET surface area was increased with decreasing the silica particle diameters. Therefore, the sample with larger surface area was attributed to absorb more blue-colored dye molecules. As seen in figure 5b, the color of dried SiO_2(15) sample changed from white to dark blue after the immersion in MB solution, indicating the physical absorption of MB by porous membranes. The rate of color change was recorded using UV-vis absorbance spectroscopy. In figure 6a, the 0.1 mM MB dye in water showed

a broad absorption band in the range of 600-700 nm, indicating the existence of the dimmer (600 nm) and monomer (660 nm) of MB [35, 36]. After the immersion of various samples in MB solutions, the intensity of MB monomer at approximately 660 nm was gradually decreased with decreasing the silica particle diameters. The intensity decreased at 2.5, 36.2 and 95 % for solutions after treatment with fibrous SiO_2(100), SiO_2(50), and SiO_2(15) membranes compared with the intensity of original 0.1 mM MB solution. However, the removing ability of resultant fibrous silica membranes for MB from aqueous solution by physical absorption is still weaker than that of silver nanoparticles doped silica nanofibers for MB by catalytic reduction reaction [37].

The wettability of a solid surface is important for various applications and is governed by both the chemistry and the geometrical microstructure of the surface [13]. FAS is a well-known low surface energy materials due to its CF groups. However, the maximum water contact angle on a flat surface that is attainable merely by lowering the surface energy with CF groups can be obtained below 120^o. Therefore, providing appropriate surface roughness is necessary to enhance hydrophobicity. The surfaces of pure inorganic fibrous silica membranes were examined to be super-hydrophilic. A conversion of surface hydrophobicity is expected using a FAS monolayer modification [30]. The FE-SEM images and surface hydrophobicity of various FAS-modified samples are shown in figure 7. After FAS modification, the fibrous silica membranes (figures 7a-c) still maintained their porous structures and rough fiber surfaces. The averaged water contact angle of FAS-modified SiO_2(15), SiO_2(50), SiO_2(100) was 167, 166, and 164^o, respectively. Additionally, all three samples showed the water-roll angles below 5^o. The surface property of fibrous silica membranes was converted from super-hydrophilic to super-hydrophobic

after FAS modification.

The FE-SEM image and surface hydrophobicity of FAS-modified sol-gel film is shown in figure 7d. It showed a flat film morphology and a water contact angle of 104^o. It was consistent with the previous report [38] that the flat films without rough surface show the water contact angle no more than 120^o. An equation ($\cos\theta` = f_1\cos\theta - f_2$) was proposed by Cassie and Baxter to describe the relationship between the water contact angle on a flat surface ($\theta$) and a rough surface ($\theta`$) composed of a solid and air [39]. Here, f_1 and f_2 are ratios of solid surface and air in contact with liquid. In other words, $f_1 + f_2 = 1$. Given the water contact angles of the FAS-modified flat silica film and the fibrous SiO_2(50) membrane, f_2 was calculated to be 0.96, which indicated that the achievement of super-hydrophobicity by FAS-modified fibrous silica membranes was mainly a result of the air trapped in the rough hierarchical micro/nanostructures of membranes.

4. Conclusion

In summary, we successfully prepared the SiO_2 nanofibrous membranes with ultra-high surface area and porosity. The colloidal silica nanoparticles with various diameters can be easily assembled into fiber shape with the template PVA via electrospinning. The results indicated that the morphology and structure of silica nanofibers were strongly affected by the silica particle diameters and solution viscosities. The silica nanofibers prepared with the smaller silica particle diameters (15 and 50 nm) were easier to maintain the continuous fiber shape than that prepared with the larger particle diameter (100 nm). Judging from the BET measurements, the BET surface areas and total pore volumes were found to be increased concurrently on decreasing the silica particle diameters. The porous silica nanofibrous membrane prepared with the smallest average particle diameter of 15 nm

showed the largest BET surface area (270.3 m^2g^{-1}), smallest pore diameter (8.8 nm), and largest total pore volume (0.66 cm^3g^{-1}). The absorption test of MB dye in water by fibrous silica membranes indicated that the fibrous SiO_2(15) membrane has the largest capacity for absorbing MB dye molecules due to its largest BET surface area among three samples. The MB dye molecule absorption capacity of fibrous silica membranes was found to be increased with decreasing the silica nanoparticle diameters from 100 to 15 nm. Additionally, the porous structures of fibrous silica membranes were proved to be effective to get super-hydrophobic surfaces after the FAS monolayer modification.

Acknowledgments

This work was partly supported by Keio Life-Conjugated Chemistry (LCC) Program of Center of Excellence (COE) Research Project in the 21st century sponsored by Japanese Ministry of Education, Science, Culture, and Sports.

References

[1] Pichonat T and Gauthier-Manuel B 2006 *Fuel Cell.* **6** 323

[2] Zhang Y Z, Feng Y, Huang Z M, Ramakrishna S and Lim C T 2006 *Nanotechnology* **17** 901

[3] Gellings P J and Bouwmeester H J M 2000 *Catal. Today* **58** 1

[4] Ding B, Yamazaki M and Shiratori S 2005 *Sensors Actuators* B **106** 477

[5] Ding B, Kim J, Miyazaki Y and Shiratori S 2004 *Sensors Actuators* B **101** 373

[6] Madhugiri S, Sun B, Smirniotis P G, Ferraris J P and Balkus K J 2004 *Micropor. Mesopor. Mater.* **69** 77

[7] Gao J, Gao T and Sailor M J 2000 *Appl. Phys. Lett.* **77** 901

[8] Halimaoui A, Oules C, Bomchil G, Bsiesy A, Gaspard F, Herino R, Ligeon M and Muller F 1991 *Appl. Phys. Lett.* **59** 304

[9] Nagel H, Metz A and Hezel R 2001 *Sol. Energ. Mater. Sol. Cell.* **65** 71

[10] Huang Z M, Zhang Y Z, Kotaki M and Ramakrishna S 2003 *Compos. Sci. Technol.* **63** 2233

[11] Onozuka K, Ding B, Tsuge Y, Naka T, Yamazaki M, Sugi S, Ohno S, Yoshikawa M and Shiratori S 2006 *Nanotechnology* **17** 1026

[12] Song M Y, Kim D K, Ihn K J, Jo S M and Kim D Y 2005 *Synthetic Met.* **153** 77

[13] Ding B, Li C R, Hotta Y, Kim J, Kuwaki O and Shiratori S 2006 *Nanotechnology* **17** 4332

[14] Miyauchi Y, Ding B and Shiratori S 2006 *Nanotechnology* **17** 5151

[15] Zeleny J 1914 *Phys. Rev.* **3** 69

[16] Zhang L and Hsieh Y L 2006 *Nanotechnology* **17** 4416

[17] Bognitzki M, Frese T, Steinhart M, Greiner A, Schaper A, Hellwig M and Wendorff J H 2001 *Polym. Eng. Sci.* **41** 982

[18] You Y, Youk J H, Lee S W, Min B M, Lee S J and Park W H 2006 *Mater. Lett.* **60** 757

[19] Li D and Xia Y 2004 *Nano Lett.* **4** 933

[20] Ding B, Kim H, Kim C, Khil M and Lee D 2003 *Nanotechnology* **14** 532

[21] Zhan S, Chen D, Jiao X and Tao C 2006 *J. Phys. Chem.* B **110** 11199

[22] McCann J, Marquez M and Xia Y 2006 *J. Am. Chem. Soc.* **128** 1436

[23] Pang M, Li D, Shen L, Chen Y, Zheng Q and Wang H 2006 *Langmuir* **22** 9368

[24] Kim C, Jeong Y, Ngoc B, Yang K, Kojima M, Kim Y, Endo M and Lee J 2007 *Small* **3** 91

[25] Shao C, Kim H, Gong J and Lee D 2002 *Nanotechnology* **13** 635

[26] Choi S, Lee S, Im S, Kim S and Joo Y 2003 *J. Mater. Sci. Lett.* **22** 891

[27] Lim J, Moon J, Yi G, Heo C and Yang S 2006 *Langmuir* **22** 3445

[28] Ding B, Kim H, Lee S, Shao C, Lee D, Park S, Kwag G and Choi K 2002 *J. Polym. Sci.* B **40** 1261

[29] Sakka S and Kamiya K 1982 *J. Non-cryst. Solids* **48** 31

[30] Ogawa T, Ding B, Sone Y and Shiratori S 2007 *Nanotechnology* **18** 165607

[31] Ding B, Kimura E, Sato T, Fujita S and Shiratori S 2004 *Polymer* **45** 1895

[32] Mukhina O, Piskunova I and Lysenko A 2003 *Russ. J. Appl. Chem.* **76** 896

[33] Tsunoda K, Umemura T, Ueno H, Okuno E and Akaiwa H 2003 *Appl. Spectrosc.* **57** 1273

[34] Saeed R, Uddin F and Summer S 2005 *Asian J. Chem.* **17** 737

[35] Matsuda N, Santos J, Takatsu A and Kato K 2003 *Thin Solid Films* **445** 313

[36] Qi L and Ma J 1998 *J. Colloid Interf. Sci.* **197** 36

[37] Patel A, Li S, Wang C, Zhang W and Wei Y 2007 *Chem. Mater.* **19** 1231

[38] Miwa M, Nakajima A, Fujishima A, Hashimoto K and Watanabe T 2000 *Langmuir* **16** 5754

[39] Cassie A and Baxter S 1944 *Trans. Faraday Soc.* **40** 546

Figure captions:

Figure 1. FT-IR spectra of (a) PVA nanofibrous membrane, (b) silica nanoparticles, (c) composite PVA/SiO_2(15) nanofibrous membrane, and (d) calcined sample of (c).

Figure 2. (a) FE-SEM image of pure PVA fibrous membrane. (b)-(d) FE-SEM images of fibrous samples formed with the average particle diameters of (b) 15, (c) 50, and (d) 100

nm. The insets are the high resolution SEM images of fibers without beads.

Figure 3. FE-SEM images of calcined silica nanofibrous membranes formed with the average particle diameters of (a) 15, (b) 50, and (c) 100 nm. The insets are the high resolution SEM images of fibers without beads.

Figure 4. FE-TEM images of calcined silica nanofibers formed with the average particle diameters of (a) 15 and (b) 50 nm. The insets are the corresponding high resolution TEM images of fibers.

Figure 5. Conventional digital camera images of (a) MB solutions after treatment with various fibrous samples and (b) the dried fibrous SiO_2(15) sample after immersion in MB solution.

Figure 6. The absorption spectra of (a) 0.1 mM MB solution and the same solution after treatment with various fibrous samples of (b) SiO_2(100), (c) SiO_2(50), and (d) SiO_2(15).

Figure 7. FE-SEM images of FAS-modified samples of (a) SiO_2(15), (b) SiO_2(50), (c) SiO_2(100), and (d) flat SiO_2 film. The insets are the corresponding profiles of a water droplet on samples.

Table 1 Solution properties and diameters of resultant fibers

Table 2 BET surface area, pore diameter, and pore volume of calcined silica nanofibers

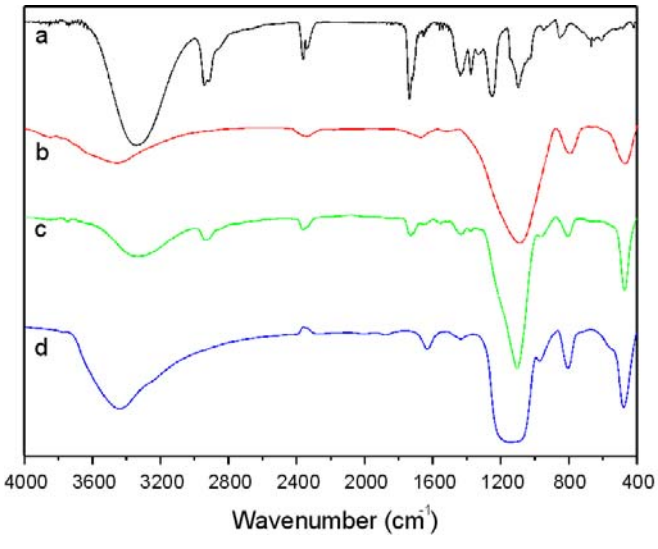

Figure 1

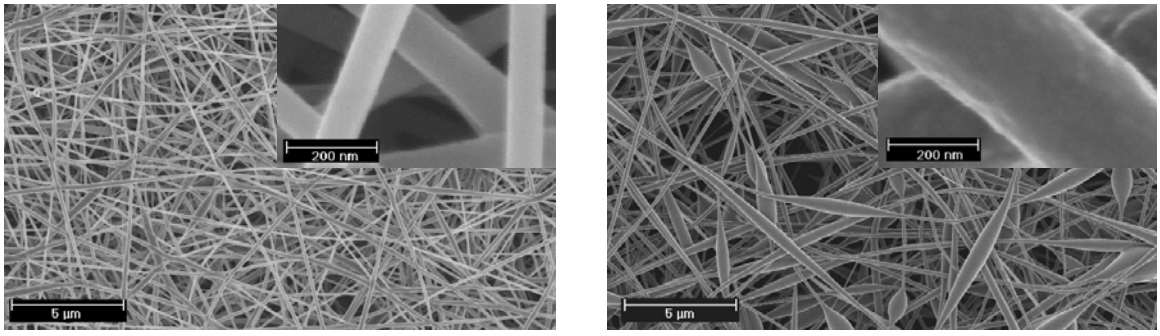

(a) (b)

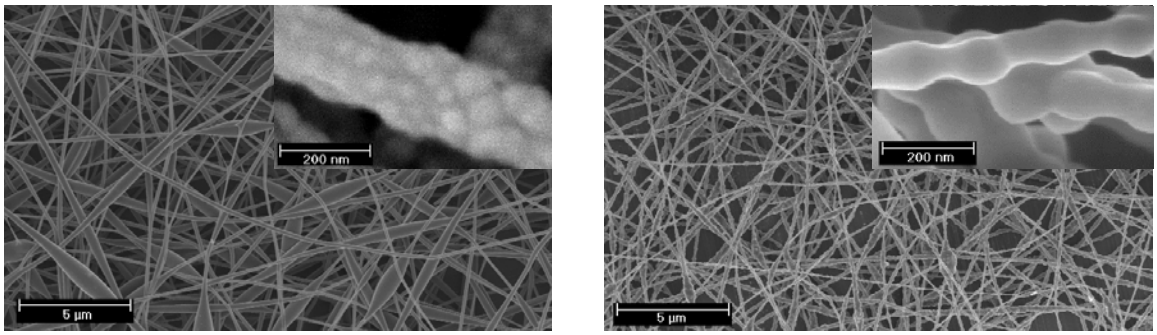

(c) (d)

Figure 2

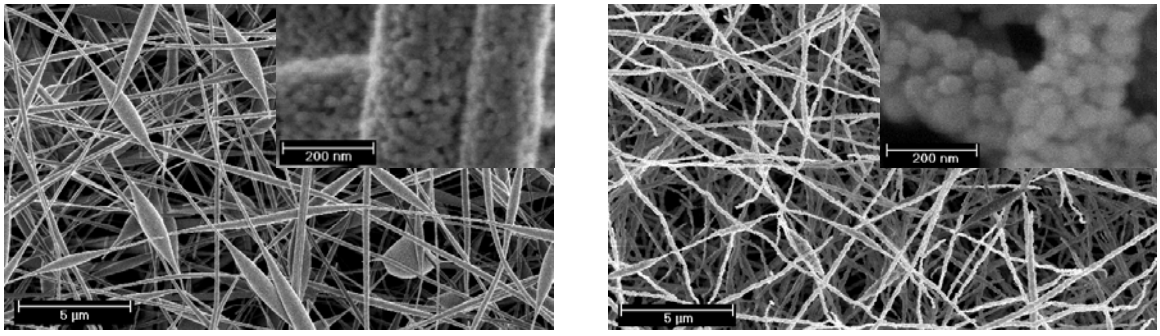

(a) (b)

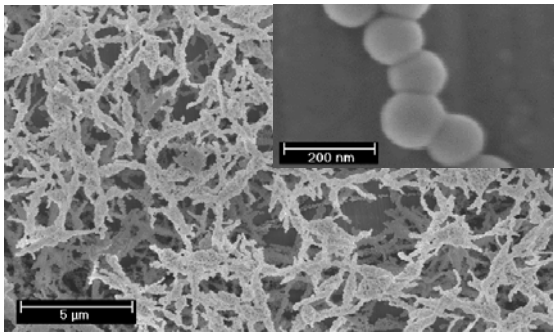

(c)

Figure 3

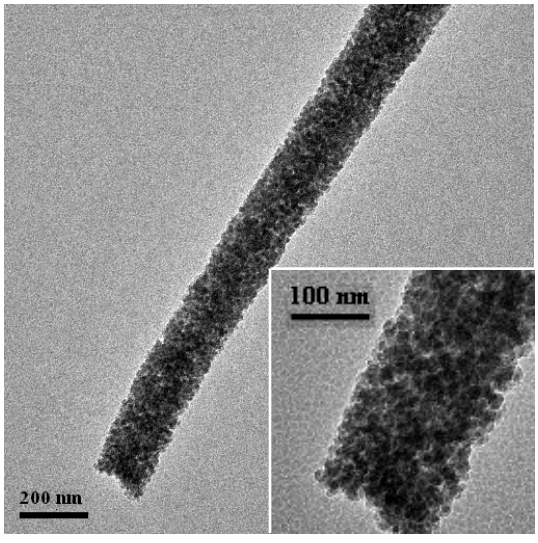

(a)

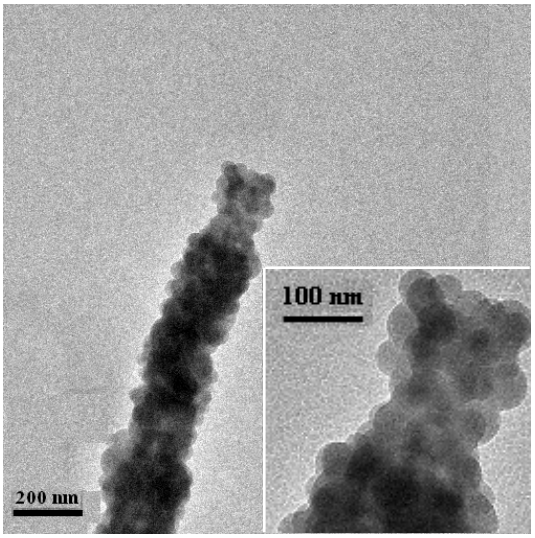

(b)

Figure 4

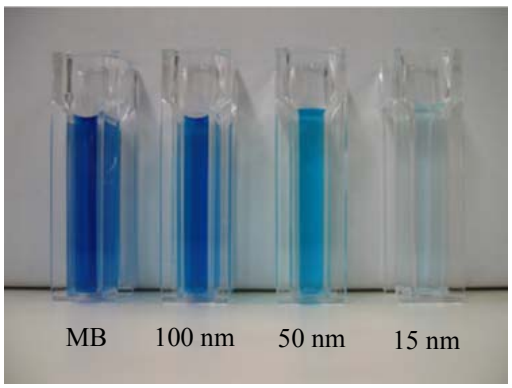

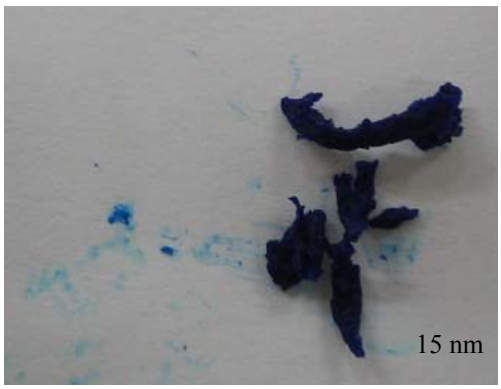

(a) (b)

Figure 5

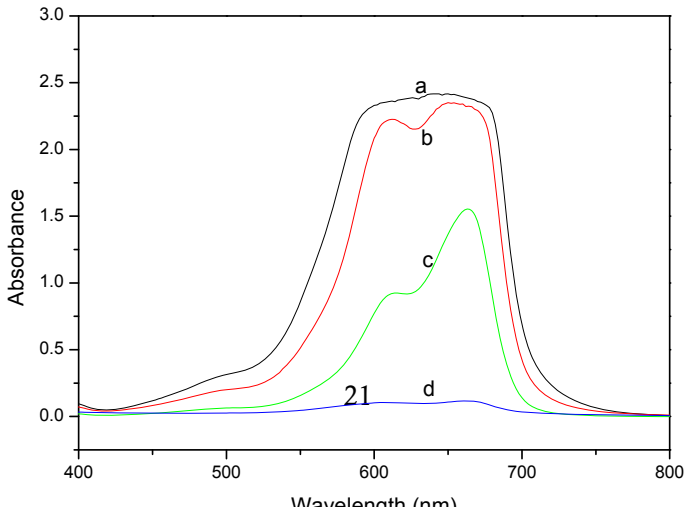
3.0
2.5
2.0
1.5
1.0
0.5
0.0
Absorbance
400
500
600
700
800
Wavelength (nm)
a
b
c
d
21

Figure 6

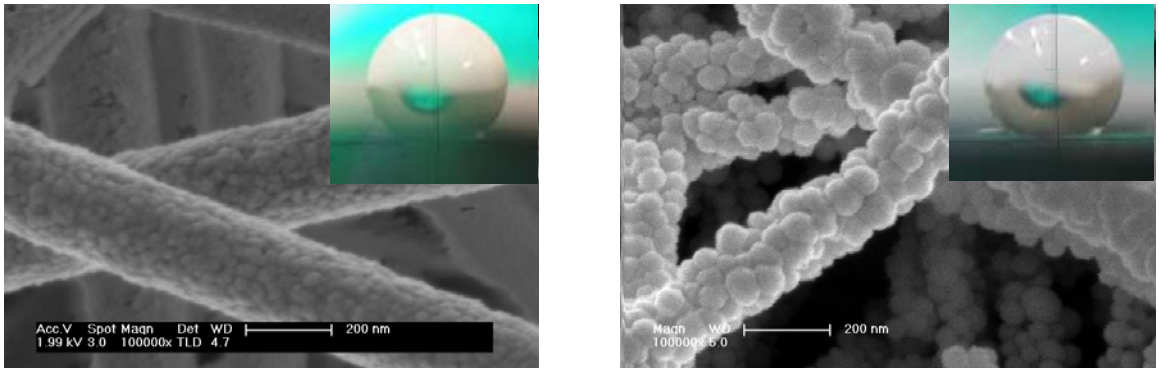
Acc.V Spot Magn Det WD 200 nm
1.99 kV 3.0 100000x TLD 4.7
Magn WD 200 nm

(a) (b)

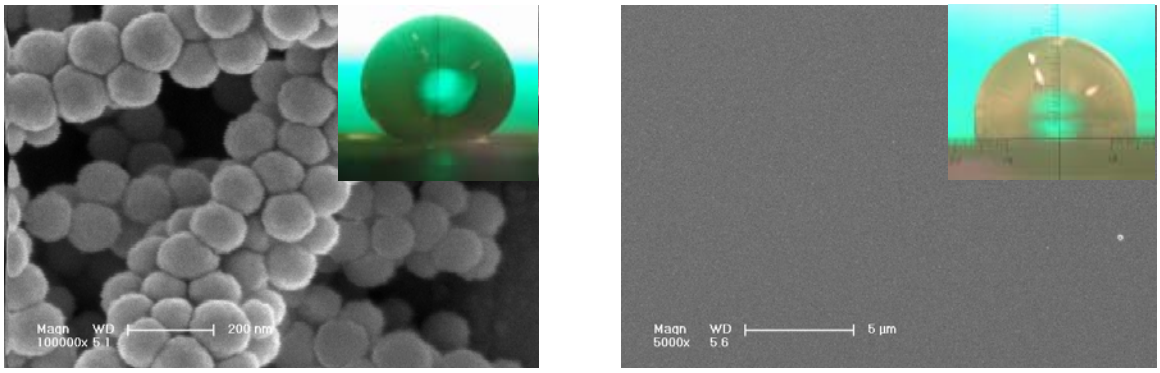

(c) (d)

Figure 7

Particle diameter (nm)	Solution composition (PVA/silica/water, wt %/wt %/wt %)	Solution Viscosity (mPas)	Fiber diameter before calcination (nm)	Fiber diameter after calcination (nm)
-	6 / 0 / 94	30	154	-
15	6 / 8 / 86	110	200	197
50	6 / 8 / 86	85	193	188
100	6 / 8 / 86	60	172	165

Table 1

Particle diameter (nm)	BET surface area (m^2g^{-1})	Pore diameter (nm)	Total pore volume (cm^3g^{-1})
15	270.3	8.8	0.66
50	64.3	25.6	0.41
100	41.4	-	0.23

Table 2